



Mapping Sensitive Vegetation Communities in Mining Eco-space using UAV-LiDAR

Bikram Pratap Banerjee^{1,2} · Simit Raval²

Received: 31 October 2021 / Accepted: 9 May 2022
© The Author(s) 2022

Abstract

Near earth sensing from uncrewed aerial vehicles or UAVs has emerged as a potential approach for fine-scale environmental monitoring. These systems provide a cost-effective and repeatable means to acquire remotely sensed images in unprecedented spatial detail and a high signal-to-noise ratio. It is increasingly possible to obtain both physiochemical and structural insights into the environment using state-of-art light detection and ranging (LiDAR) sensors integrated onto UAVs. Monitoring sensitive environments, such as swamp vegetation in longwall mining areas, is essential yet challenging due to their inherent complexities. Current practices for monitoring these remote and challenging environments are primarily ground-based. This is partly due to an absent framework and challenges of using UAV-based sensor systems in monitoring such sensitive environments. This research addresses the related challenges in developing a LiDAR system, including a workflow for mapping and potentially monitoring highly heterogeneous and complex environments. This involves amalgamating several design components, including hardware integration, calibration of sensors, mission planning, and developing a processing chain to generate usable datasets. It also includes the creation of new methodologies and processing routines to establish a pipeline for efficient data retrieval and generation of usable products. The designed systems and methods were applied to a peat swamp environment to obtain an accurate geo-spatialised LiDAR point cloud. Performance of the LiDAR data was tested against ground-based measurements on various aspects, including visual assessment for generation LiDAR metrics maps, canopy height model, and fine-scale mapping.

Keywords Upland swamps · Mine surveying · Monitoring · Environment sustainability · Drones and laser scanning

1 Introduction

Extraction and use of minerals is a critical component in the development of current and future societies. In contrast to its benefits there have been concerns about the negative impacts of mining on the society and the environment. Mining is a temporary use of the land, but its socio-environmental impacts could be long term. Continuous monitoring

of the mine environment provides an opportunity for early remediation leading to the long-term sustainability of the environment and mining operations.

1.1 Coal mining under upland peat swamp environments

Mining under economically significant and ecologically sensitive environments such as upland peat swamps pose a unique challenge to the mining industry and government regulators. Upland peat swamps in the Sydney basin bioregion, New South Wales, Australia mainly occur on coastal highland or upland plains of Triassic Sandstone formation (Department of Sustainability, Environment, Water, Population and Communities, 2018) and are technically termed temperate highland peat swamps on sandstone (THPSS). THPSS consists of uniquely diverse ecosystems comprising treeless heaths and sedgelands. These environments play an essential role in filtering and slowly releasing water to

✉ Simit Raval
simit@unsw.edu.au

Bikram Pratap Banerjee
bikram.banerjee@agriculture.vic.gov.au

¹ Agriculture Victoria, Grains Innovation Park, 110 Natimuk Road, 3400 Horsham, VIC, Australia

² School of Minerals and Energy Resources Engineering, University of New South Wales, 2052 Sydney, NSW, Australia

downstream watercourses. Additionally, providing habitats for a wide range of animals, including birds, reptiles and frogs. A few of the threatened species with habitat requirements specific to THPSS conditions include the Giant burrowing frog (*Heleioporus australiacus*), Blue Mountains water skink (*Eulamprus leuraensis*) and Giant dragonfly (*Petalura gigantea*) (CoA 2014). THPSS environments are listed as an endangered ecological community because of their limited distribution and vulnerability to ongoing threats such as underground longwall mining and agriculture (CoA 2014). These ecological communities may be influenced by underground longwall coal mining activities, which can potentially disrupt the local geology, topography, water regimes and water quality of the THPSS (NSWDP 2008; CoA 2014; Vervoort 2021). Potential impacts include the disruption of water availability and quality, leading to the degradation of the host ecosystem.

Accidental discharge of mine wastewater into drainage lines uphill from the swamps is also a potential risk (CoA 2014). Improperly treated mine water discharges include saline discharges (Opitz and Timms 2016; Greene et al. 2016) and acid mine drainage (Akcil and Koldas 2006), all of which can degrade freshwater resources and potentially impact sensitive environments and ecosystems (Younger and Wolkersdorfer 2004). Poor water quality may involve one or more parameters: salinity, turbidity, acidity, metals, organics, and other contaminants of concern, such as toxic algae or radiological elements. However, it is difficult to be

definitive about water quality and identify potential short and long-term impacts on swamps with limited monitoring.

1.2 Existing monitoring technologies

Several traditional methods are used for monitoring the potential impact of mining on peat swamps. Methods suitable for early identification of effects include field-based geotechnical methods (borehole testing and joint monitoring), geophysical methods (downhole logging, electromagnetic conductivity and ground-penetrating radar) and hydrological methods (shallow groundwater monitoring, deep groundwater level or pressure monitoring) (CoA 2014). However, peat swamps are often located in steep and elevated terrain. Many field-based methods are constrained by difficult site access and coverage area, mainly if heavy equipment is necessary. The status of swamps can also be assessed using baseline ecological conditions, which include vegetation survey (flora census, vegetation community patterns and vegetation condition), fauna (wetland frog, reptile, bird and invertebrate) monitoring, and invasive species monitoring methods (CoA 2014). These ecological field surveys are limited to monitoring specific locations and rely on data extrapolation. These methods are also subjective to the approach used to infer the ecological baselines. Usually, a set of different ecological surveying methods are needed to establish the condition of swamps.

Remote sensing based methods are alternative approaches to monitoring the ecological response of swamp vegetation.

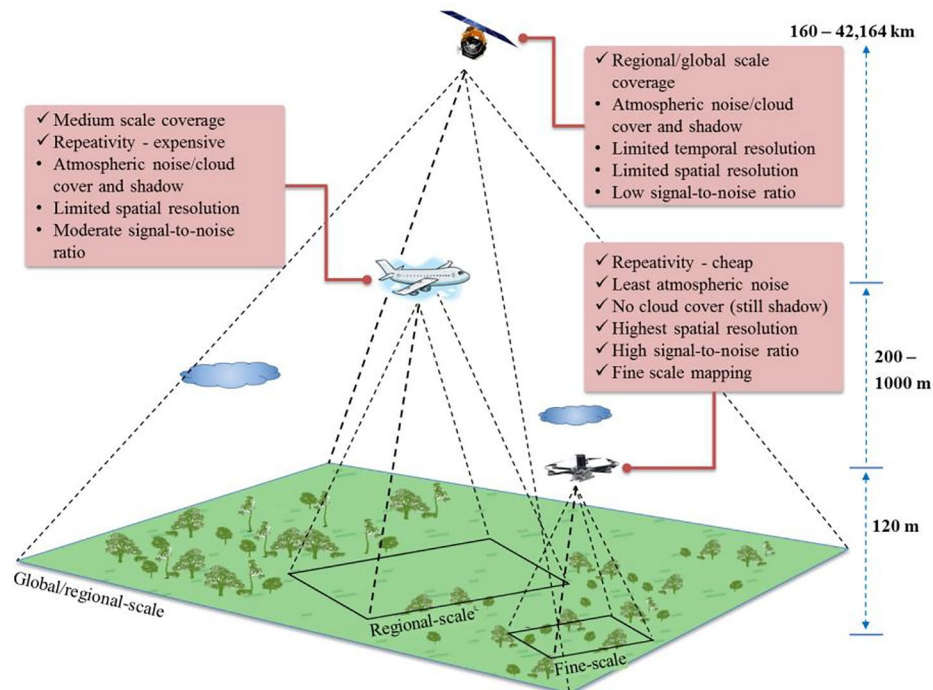


Fig. 1 A comparison of satellite, airborne and uncrewed aerial vehicle (UAV) remote sensing systems for environmental monitoring applications

These methods involve passive (multispectral, hyperspectral and thermal) and active (light detection and ranging, i.e. LiDAR and radar) sensing approaches from airborne and satellite systems. Multispectral indices, such as the normalised difference vegetation index (NDVI), indicate vegetation vigour, or greenness, assuming that high chlorophyll absorption in plants conveys information on plant health (Gandaseca et al. 2009; Setiawan et al. 2017). The enhanced vegetation index (EVI) has advantages over the NDVI in accurately interpreting vegetation coverage by incorporating corrections for atmospheric and soil influences (Weier and Herring, 2000). Time series EVI data is available in high frequency and has been used for monitoring the dynamics of peat swamps (Setiawan et al. 2016). Changes in vegetation distribution within peat swamps can be observed using high-resolution remote sensing (Jenkins and Frazier 2010; Zhang et al. 2018). Light detection and ranging (LiDAR) is an active-sensing system that can differentiate between bare earth and 'non-ground' points such as vegetation to monitor biomass (Englhart et al. 2013). The insufficient spatial resolution of aerial and satellite based methods also restricts fine level assessment of vegetation conditions in THPSS. Consequently, existing studies (Jenkins and Frazier 2010) have been limited to delineating swamp boundaries and vegetation baseline estimations.

1.3 Environmental monitoring using UAVs

Plant species physiologically adapted to survive in periodically inundated conditions have a competitive advantage in wetlands and swamps. Any alteration in swamp hydrology that causes drying of the peat will reduce this competitive advantage of wetland species and allow species assemblages to shift towards more terrestrial vegetation types (CoA 2014). Increases in the proportion of terrestrial species in a swamp may indicate changing swamp hydrology. No change in the proportion of terrestrial species (or change within equilibrium limits) indicates the stability of hydrology and peat moisture levels. This baseline composition of species within the equilibrium limit is regarded as the characteristic vegetation composition, which is unique for each environment, including THPSS. Identification of individual vegetation species or assemblages in THPSS is critical to characterise their vegetation composition, and is the first step towards monitoring the changing health of the micro-ecosystem under natural or anthropogenic stresses (Banerjee et al. 2017, 2020).

1.4 UAV-LiDAR scanning in environmental monitoring

Recent developments in the miniaturisation of aerial robotic platforms and electro-optical sensors have established a new era of aerial remote sensing using uncrewed aerial vehicles (UAVs). The unprecedented resolution, high signal-to-noise ratio, operational flexibility, ability to access remote locations, ease of use and low cost have attracted interest from scientific and commercial communities (Colomina and Molina 2014; Ren et al. 2019). Such features make them suitable for fine-scale environmental monitoring than satellite or airborne systems (Fig. 1). UAVs with optical and infrared cameras have been used in THPSS; however to date, the approach has been limited to the detection of a single species (*Gleichenia dicarpa*) (Strecha et al. 2012) and the mapping of vegetation community boundaries (Lechner et al. 2012). Studies were undertaken to test the potential of a UAV-hyperspectral system to map five swamp species (*Allocasuarina littoralis*, *Empodisma minus*, *Lepidosperma limicola*, *Lepidosperma neesii* and *Pteridium aquilinum*) in THPSS environments (Banerjee et al. 2020; Banerjee and Raval 2021). These studies demonstrate the advantage of both high spatial and spectral resolutions for effectively assessing vegetation in spectrally complex swamp environments.

UAV-LiDAR system is a cutting-edge technology that is and finding increased use in different applications. Jaakkola et al. (2010) developed and demonstrated the potential of a UAV-LiDAR system in a forestry application. Integration of lightweight LiDAR sensors with rotary type UAVs provided the benefit of using them more effectively in restricted environments to obtain high-resolution 3D datasets at unprecedented detail. The high density of the LiDAR datasets directly translates to the accuracy of the derived secondary products such as topographic (Lin et al. 2011) and vegetation (Wallace et al. 2014) metrics. Banerjee et al. (2018) used optical imaging data and structural metrics from UAV-LiDAR for mapping complex vegetation communities in upland peat swamps. Therefore, accurate estimation of these structural metrics is crucial to environmental applications such as generation of topographic and canopy models, identification of vegetation types and attributes such as leaf area index. Finally, UAV-LiDAR systems are accurate, easy to use and have lower operational costs than traditional airborne laser scanning surveys, making them suitable for recurrent use in environmentally sensitive areas for condition assessment and reporting.

To this end, this study focuses on using a UAV-LiDAR system in mapping sensitive vegetation communities in a coal mining area. The work involved detailed protocols of (1) collecting UAV-LiDAR data, including procedures for

filtering and generating a coherent point cloud, (2) processing to generate structural metrics, (3) generating the canopy height model, and (4) classification of sensitive vegetation communities using different algorithms.

2 Materials and methods

2.1 Study area and identification of vegetation of interest

Temperate highland swamps on sandstone (THPSS) are critically endangered ecosystems (CoA 2014) distributed in the Blue Mountains, Lithgow, Southern Highlands and Bombala regions in New South Wales, Australia. This study focused on two swamps in a THPSS site in the Southern Highlands, located near Wollongong, southwest of the city of Sydney, Australia.

The two swamps have a complex distribution of several species and vegetation communities, which exist as

shrub-type vegetation thickets (*Banksia* and *Tea-tree*), and Sedgeland-Heath complexes (Cyperoid, Restioid and Sedgelands) (NPWS, 2003; Jenkins and Frazier 2010). The selection of species for a vegetation monitoring and classification study needs to consider the ability to map the vegetation components (or classes) and their ecological significance. A total of eight vegetation classes were selected with five swamp vegetation classes and three non-swamp vegetation classes. A set of five swamp vegetation classes were identified based on their abundance and sensitivity to anthropogenic impacts: Dagger hakea (*Hakea teretifolia*), Grass tree (*Xanthorrhoea resinosa*), Pouched coral fern (*Gleichenia dicarpa*), Heath-leaved banksia (*Banksia ericifolia*), and Sedgeland complex (*Empodisma minus*, *Gymnoschoenus sphaerocephalus*, *Lepidosperma limicola*, *Lepidosperma neesii*, *Leptocarpus tenax* and *Schoenus brevifolius*). Presence of certain non-swamp or terrestrial vegetation species can indicate potential alteration of swamp hydrology. Therefore, a set of three non-swamp vegetation classes were also identified: Black sheoak (*Allocasuarina littoralis*), Bracken

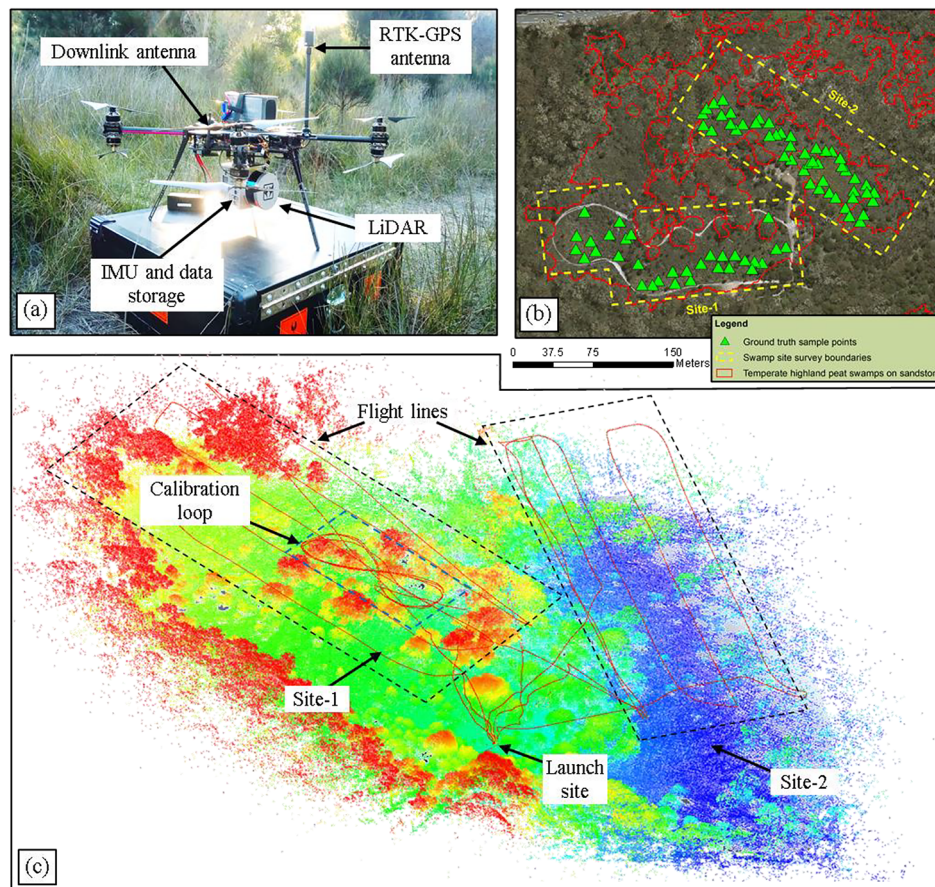


Fig. 2 **a** The integrated UAV-LiDAR system used in the study environment, **b** Map view of the study area with a detailed view of the swamp site survey boundaries (site-1 and site-2), ground truth sample locations (green triangles) and THPSS boundaries, and **c** 3D subsampled point cloud view with the calibration loop and flight lines for data acquisition

fern (*Pteridium aquilinum*), and *Eucalyptus* trees. The list of classes and corresponding species was identified through several field campaigns and consultation with expert advice from field ecologists.

2.2 Sampling design and field measurement

Ground truth data includes a set of labels on the images intended for defining a model for classification or parameter retrieval. A proper ground truth sampling strategy is essential to eliminate significant biases from leaking into the process (Congalton 1991). Furthermore, to ensure that the ground data is representative of the spatial population, a suitable sample design must be chosen. Stratified random sampling is a method of selecting in which the elements of the population are allocated into sub-populations (e.g. strata) before the sample is taken, and then each stratum is randomly sampled (Brogaard and Ólafsdóttir, 1997). This sampling approach is used when specific information about certain sub-populations and increasing precision of the estimates for the entire population is desired (Cochran, 1977; Clark and Hosking, 1986). In this study, a similar stratified sampling approach has been used. A total of 80 locations for ground truth sample collection were identified using this sampling approach within the shrub-type swamp vegetation classes only (i.e. Grass tree, Pouched coral fern and Sedgeland complex) for the field survey, i.e. a total of 32 locations for swamp site-1 and 48 locations for swamp site-2 (shown as green triangles in Fig. 2b). Coordinates of each location were measured using the ground-based real-time kinetic – differential global positioning system RTK-DGPS unit (Leica Viva GS15 GPS system) within 3 mm of absolute accuracy. A set of four discrete ground truth points was identified at 1 m distances in the North, East, South and West directions using a compass as reference. This produced a total of $80 \times 4 = 320$ ground truth points for the shrub-type swamp vegetation. For each ground truth point, the vegetation's species composition and canopy height were recorded.

Canopy Height Measurement – The canopy height was measured using the vertical graduated scale with a pointed bottom end. Due to the varying degree of density, in areas of high compaction of the shrub-type swamp vegetation, it was challenging to ensure that the bottom end of the graduated scale reached the true soil surface. Therefore, several sets of measurements were taken within (50 cm) of the vicinity of the sampling point to identify the canopy height correctly. In areas of highly fragile canopies several measurements (5 to 10) were collected within (50 cm) the vicinity of the point, and the median value was used as the representative measurement.

2.3 UAV-LiDAR scanning

This section describes the method of developing a UAV-LiDAR system and workflow, including a description of the LiDAR sensor used, procedures for system integration and aerial data acquisition, conversion of raw data to point cloud and pre-processing of the generated point cloud.

2.3.1 LiDAR sensor

This study used a mobile integrated LiDAR system (Phoenix Aerial Scout). The primary sensor onboard the UAV is a Velodyne PUCK LiDAR scanning system. The internal laser sensor has a maximum range of 120 m and a range of 80 m at 60% target reflectivity, which produces a typical range accuracy of ± 3 cm with a range resolution of 2 mm. The laser sensor records ranges and intensities for up to two echoes per pulse. It has a rectangular aperture beam width of 9.5 mm (vertical) \times 12.7 mm (horizontal) and a beam divergence of 0.07° (vertical) \times 0.18° (horizontal). The scanner uses a rotating sensor scanning mechanism with 16 lasers oriented on a vertical axis. In this configuration the sensor has an angular FOV (vertical) of $\pm 15.0^\circ$ (30°) and angular resolution (vertical) of 2° . The laser sensors spin on a horizontal axis with a 5–20 Hz rotation rate to produce an angular FOV (horizontal) of 360° and angular resolution (horizontal) of 0.1° – 0.4° . The scanner has characteristic beam divergence more suitable for an automotive application and less ideal for a mapping sensor. Nevertheless, this enables low power consumption and lightweight (830 g) to allow its use on UAV platforms.

The remaining sensors within the integrated LiDAR sensing payload consist of a dual-frequency RTK-GPS/GLONASS with a lightweight antenna and inertial measurement unit (IMU). The measurements from the GPS and the IMU are synchronised with a precision internal clock. To achieve the highest possible accuracy, they are logged at a rate of 50 Hz onto an embedded computer with a data storage unit. These core components and wirings (except the GPS antenna) are housed inside a protective harness and fastened to the LiDAR sensor using screws. The sensor records 0.3 million laser points per second on the on-board computer and downlinks a subsampled point cloud data to the ground station in real-time through a 5.8 GHz long-range Wi-Fi wireless system to avoid acquisition errors. The total payload weight of the integrated LiDAR system is 1.6 kg, and the dimensions are 16 cm \times 11.6 cm \times 11.6 cm.

2.3.2 System integration and aerial data acquisition

The integrated LiDAR sensing system was mounted onto a UAV with the vertical axis of the LiDAR sensor aligned to

the along-track and horizontal rotating plane aligned in the across-track direction of the flight trajectory. A customised coaxial rotor quadcopter UAV system was used to mount the integrated LiDAR sensing payload. Platform instability and vibration of the UAV platform is a critical issues for LiDAR data acquisition. High-frequency vibrations produced from the rotor movements of modern UAV platforms can induce rapid movement, which is difficult for the IMU to compensate for. The quadcopter assembly provided necessary stability, and the coaxial rotor configuration reduced vibration due to aerodynamic compensations, which further increased the total lift weight capacity of the UAV. Vibration from rotors was further isolated by mounting the LiDAR payload system using four silicon rubber mounts. This provided sufficient physical support and compensation for the system to acquire precise point cloud data. The total system weighed under 9 kg and offered a flight time of around 15 min. The integrated UAV-LiDAR system is shown in Fig. 2a.

The customised coaxial quadcopter has a standalone control system based on a 3DR Pixhawk2 mini flight controller. A pre-survey initialisation procedure was performed, which required the UAV-LiDAR system to be powered on and then flown three times in a pattern of “8” to calibrate all the time-base mismatches between IMU, GPS and laser scanner. The procedure is highlighted with a blue-dashed-bounding box in Fig. 2c. The UAV-LiDAR system was operated over the two test sites according to a pre-designed flight plan with a flying height of 50 m and speed of 5 m/s, with a transect spacing of 20 m. In this flying configuration, each test site was covered with a set of four parallel flight transects, and the entire mission was completed in two separate flights, which took approximately 25 min in total.

2.3.3 Raw data to point cloud

All the raw ranging information from the laser scanner, along with the time-tagged roll, pitch, yaw and position information from the IMU and RTK-GPS/GLONASS units, was downloaded from the on-board data storage. The raw laser scanner data consists of a ‘.ldr’ format file of the range records. The orientation and positioning data were logged on a separate file. The raw datasets were fused using a standard range transformation model (in Phoenix Aerial Spatial Fuser v3.0.5) to produce the georeferenced point cloud (in log ASCII or ‘.las’ format). The process included correction for the centre of the IMU, RTK-GPS/GLONASS unit to the laser sensor geometric translation. All 16 channels of the LiDAR were used for the generation of the point cloud. The laser footprint at nadir was 0.12 m along-track and 0.31 m across-track with a flying height of 50 m. To limit laser beam divergence, laser returns with ranging values > 60 m were masked out in point cloud generation. With the spacing

between transects at 20 m, the resultant point had a swath width of 66.3 m and a lateral scan overlap of approximately 70%. This resulted in significant overlap of laser footprints in both along and across-track directions and provided sufficient angularity to the measurements to scan further inside the tall tree canopies.

Accurate sensor localisation and orientation measurements are crucial for direct georeferencing, as these parameters are not consistent throughout the UAV-LiDAR survey. A set of time dynamic quality threshold parameters was used to avoid error propagation into the final point cloud model due to positional or orientational uncertainties. According to this criterion, for the small durations when the quality parameters were poor such as uncertainty in altitude > 10 cm, position error > 10 cm, number of available satellites < 9, and differential lag > 20 ms, the raw data to point cloud transformation was avoided.

2.3.4 Pre-processing – point cloud sampling, segmentation and height filtering

A LiDAR scan often contains tightly placed points that are redundant in nature. These points could be left behind due to oversampling caused by the high sampling rate of the scanner or by the overlap of the point cloud from multiple transects. Such redundant points from the UAV-LiDAR point cloud were removed by sampling the data with a minimum threshold (> 0.01 m) separation criterion. Minor errors introduced by the IMU or RTK-GPS system can cause some erroneous points to be produced in a LiDAR scan that is outside the general body of the scanned surface. A point cloud segmentation approach using connected component labelling (in CloudCompare v2) was applied with an 8th level octree and 10,000 connected points to identify the primary segment of the scanned surface and remove non-surface erroneous points. Further processing was performed to filter the point cloud into ground and non-ground (vegetation) classes and to calculate the heights of the vegetation points above the ground using the BCAL (BCAL LiDAR Tools for ENVI) height filtering tool (Streutker and Glenn 2006). The parameters for canopy spacing were set at 5 m with a maximum vegetation height of 30 m in the processing step, which represented the vegetation canopy structure of *Eucalyptus* trees around the swamp environment. The pre-processing steps also helped filter out erroneous artefacts which would otherwise propagate to the results.

A surface point density map was produced after essential pre-processing (point cloud sampling, segmentation and height filtering) to test the quality of the resulting point cloud, i.e. to identify if the number of scanned points was sufficient and if a moreover uniform point distribution exists throughout the study area, which is essential for generation

Table 1 Derived LiDAR metrics from the point cloud scan of the swamp environment

Derived LiDAR metrics	Item	Description
Topographic	Absolute roughness	The roughness (standard deviation) of all elevation points within each pixel
	Local roughness	The roughness (standard deviation) of all elevation points within each pixel after the local slope has been removed (de-trended)
	Slope	The average slope of all points within each pixel in degrees
	Aspect	The aspect of the average slope of all points within each pixel in degrees from North
	Topographic solar radiation index (TRASP)	Transformation of aspect (TRASP), used by (Roberts and Cooper, 1989), is defined as $[1 - \cos((\pi/180)(aspect - 30))] / 2$. TRASP assigns the low value to north-northeastern aspect, and the high values to, dryer south-southwesterly slopes
	Slope cosine aspect (Slpcosasp)	Slpcosasp is calculated as $slope \times \cosine (aspect)$ (Stage, 1976).
	Slope sine aspect (Slpsinasp)	Slpsinasp is calculated as $slope \times sine (aspect)$ (Stage, 1976).
	Point density	The density of all points within each pixel
Vegetation Products	Minimum height	The minimum of all height points within each pixel
	Maximum height	The maximum of all height points within each pixel
	Height range	The difference of maximum and minimum of all height points within each pixel
	Mean height	The average of all height points within each pixel
	Median absolute deviation (MAD) from median height	The MAD value of all height points within each pixel. $MAD = 1.4826 \times median (height - median height)$
	Mean absolute deviation (AAD) from mean height	The AAD value of all height points within each pixel. $AAD = mean (height - mean height)$
	Height variance	The variance of all height points within each pixel
	Height standard deviation	The standard deviation of all height points within each pixel. This is also called 'absolute vegetation roughness'
	Height skewness	The skewness of all height points within each pixel
	Height kurtosis	The kurtosis of all height points within each pixel
	Interquartile range (IQR) of height	The IQR of all height points within each pixel. $IQR = Q_{75} - Q_{25}$, where Q_x is x^{th} percentile
	Height coefficient of variation	The coefficient of variation of all height points within each pixel
	Height percentiles	The 5th, 10th, 25th, 50th, 75th, 90th and 95th percentiles of all height points within each pixel
	Number of LiDAR returns	The total number of all points within each pixel
	Number of LiDAR vegetation returns (nV)	The total number of all the points within each pixel that are above the specified crown threshold value (CT)
	Number of LiDAR ground returns (nG)	The total number of all the points within each pixel that are below the specified ground threshold value (GT)
	Total vegetation density	The percent ratio of vegetation returns and ground returns within each pixel. $Density = nV/nG * 100$
	Vegetation cover	The percent ratio of vegetation returns (nV) and total returns within each pixel
	Percent of vegetation in height range	Percent of vegetation in height ranges 0–1 m, 1–2.5 m, 2.5–10 m, 10–20 m, 20–30 m, and > 30 m within each pixel. $Percent\ of\ Vegetation = \frac{Number\ of\ vegetation\ returns\ in\ the\ range}{Total\ vegetation\ returns}$
	Canopy relief ratio	Canopy relief ratio of points within each pixel. $Canopy\ relief\ ratio = \frac{(H_{mean} - H_{min})}{(H_{max} - H_{min})}$
Texture of heights	Texture of height of points within each pixel, i.e. standard deviation of height above ground threshold and height below crown threshold	
Foliage height diversity (FHD)	is denoted by $FHD = -\sum p_i \ln(p_i)$ where p_i is the proportion of the number of LiDAR returns in the i^{th} layer to the sum of LiDAR points of all the layers (using all points)	
Foliage height diversity above ground threshold (FHD _{GT}) – points above ground	FHD calculated only using points above GT	
Intensity	Minimum Intensity	The point with the minimum intensity value within each pixel
	Maximum Intensity	The point with the maximum intensity value within each pixel
	Mean Intensity	The mean intensity of all points within each pixel
	Standard Deviation Intensity	The standard deviation of intensity value of all points within each pixel

of useful metrics from the point cloud. The surface point density map was produced by counting the number of points scanned over a regularly spaced grid of 1 m throughout the study area. Additionally, a histogram distribution of the surface point density was produced to identify the point density of the scan.

2.3.5 Retrieval of LiDAR metrics

The relative position or local relationships between a set of neighbourhood points in a LiDAR point cloud can be mathematically analysed to derive a spatially representative surface map which is easier to use with traditional remote sensing tools. These mathematical derivatives are known as LiDAR metrics. A total of 35 LiDAR metrics related to topography, vegetation, and intensity were derived using BCAL LiDAR Tools (Table 1).

Generation of LiDAR metrics from a highly dense point cloud acquired from UAV-LiDAR is a computationally intense and time-consuming process, particularly in the absence of a graphics processing unit (GPU) based on multi-core parallel processing capabilities with BCAL. Therefore, LiDAR metrics (Table 1) generation was processed at a grid size or pixel resolution of 10 cm to limit excessive processing time. The metrics were derived with a ground threshold of 10 cm and a crown threshold of 20 cm. A bin height of 1 cm was used to compute foliage height density (FHD) parameters.

2.3.6 Extracting canopy height model from LiDAR data

A bare earth digital elevation model (DEM) at 10 cm resolution was produced using the LiDAR point cloud by only considering the last returns in BCAL. The process assigns the minimum altitude value of the previous return points within each grid or pixel size of 10 cm. The model approximates a DEM surface by interpolation in dense areas with the absence of correct ground-level measurements due to dense canopies. A digital surface model (DSM) was also computed by using the first returns of the LiDAR point cloud, and assigning the maximum altitude value of any point within the 10 cm grid to the corresponding pixel value of the DSM. The canopies of shrub-type swamp vegetation are often fragile or tilted (due to wind), which usually does not produce sufficient first return measurements for correct canopy height measurements. A 5×5 local maximum filter was applied on the DSM to assign the maximum height within an area of 50 cm by 50 cm to the central pixel. A canopy height model (CHM) was then measured by subtracting the DEM from the filtered DSM. The accuracy of the canopy height model was validated against the field-based measurements of canopy height of shrub-type vegetation

using the coefficient of determination (R^2) statistics (Cameron and Windmeijer 1997).

2.3.7 Classification of LiDAR data for mapping

The stacked LiDAR metrics were used to differentiate the different types of swamp vegetation classes. A set of seven supervised classifiers such as parallelepiped (PP), maximum likelihood (ML), minimum distance (MD), Mahalanobis distance (MHD), spectral angle mapper (SAM), spectral information divergence (SID), and support vector machine (SVM) were used from ENVI (Exelis Inc., Harris Corporation, Boulder, Colorado, United States) to demonstrate the ability of the different datasets in the classification process and cross-validation. To mutually evaluate the classifiers, a standard 'null' parameter setting was used for each classifier, i.e., no standard deviation threshold from mean was used for PP, MD and MHD, no probability threshold was used for ML, no maximum threshold angle for the SAM, and no maximum divergence angle was used for SID. The SVM classifier out of the set of seven classifiers is based on machine learning, and as such, was computationally intensive. However, the objective here was not to identify an efficient and robust classification workflow but to evaluate the potential of LiDAR data in mapping sensitive vegetation communities with well-established classification methodologies. A standard parameter setting using a radial basis function with a kernel gamma function of 0.167, penalty parameter of 100 and pyramid level of 5 was used.

The 35 LiDAR metrics (Table 1) were first stacked to produce a composite multi-dimensional dataset. However, all the derived LiDAR metrics do not necessarily contain useful information for classification. Therefore, two data dimensionality reduction techniques – principal component analysis (PCA) (Richards and Richards 1999) and independent component analysis (ICA) (Hyvärinen and Oja 2000) were used to condense the information content of 35 LiDAR metrics. This step essentially condensed the useful information from all the 35 metrics to the initial layers of the stacked dataset. The first 15 LiDAR metrics with high information content were then selected from the stacked dataset, where the eigenvalues > 0.2 . A 3×3 enhanced frost filter (Lopes et al. 1990) was used to adaptively average pixel values in homogenous clusters with a coefficient of variation, $C_u=0.523$, and an impulse response convolution kernel for heterogeneous clusters with a maximum coefficient of variation, $C_{max}=1.732$. At this stage, the dimensionally reduced and filtered 15 metrics composite data can undergo a classification operation similar to the multispectral and hyperspectral datasets.

A total of 320 ground truth measurements were collected for shrub-type swamp vegetation through a rigorous field

survey, the vegetation class for each point was geospatialised as a field attribute. A buffer with a radius of 5 cm was created around each of the 320 measurements to produce an equivalent ground truth polygon for each measurement. An additional 128 ground truth polygons were also created through visual interpretation of high-resolution optical data maps. Ground truth samples for bush or tree-type vegetation classes such as Dagger hakea, Heath-leaved banksia, Black sheoak, and *Eucalyptus* trees were primarily acquired using this approach. The sampled ground-based (320) and image-based (128) polygons were randomly divided into 1:1 mutually exclusive training and test samples, i.e. 160 ground and 64 image-based polygons for each training and test group. The ground truth training set was used to train the classifiers, and the test samples were used to compute the overall accuracy (OA), kappa (κ) and confusion matrix to evaluate the classification accuracies. All the seven classifiers were applied to the datasets at 10 cm resolution, and the overall accuracy (OA) and kappa (κ) values were tabulated. Classification maps based on the best classifier performance and the corresponding confusion matrix were produced.

3 Results

3.1 Geometric quality assessment for UAV-LiDAR

The UAV-LiDAR system and the raw data to the point cloud processing segment produced a georeferenced point cloud. The accuracy of the UAV-LiDAR metrics obtained through the processing chain was tested against referenced optical maps. The point cloud achieved an average error of 10.4 cm, which was deemed sufficient for further environmental monitoring applications. For the study area, a UAV-LiDAR point cloud with a surface height profile for a portion of the study area is shown in Fig. 3.

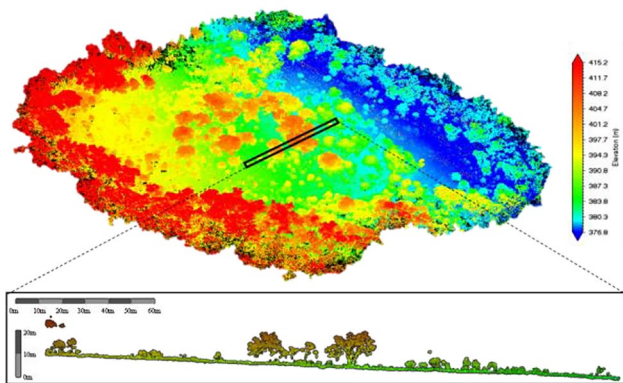


Fig. 3 Point cloud obtained through UAV-LiDAR survey of the study area with a cross-section view of the surface height profile for a portion the swamp

3.2 Surface point density and effect of pre-processing

A uniform surface density map is essential for accurate processing and generating higher-order products from the LiDAR point cloud, such as LiDAR metrics. The programmed flight plan of the LiDAR scan produced a more uniform distribution of points. The point cloud was further processed to filter out redundant points, which improved the uniformity of the point cloud. This facilitates a moreover uniform distribution of surface point density, which helps avoid density induced bias in the computation of LiDAR metrics. The calculated surface point density map for the study area is shown in Fig. 4a. A high density of point cloud is also essential for accurate fine-scale mapping applications. A histogram of the surface point density plot is shown in Fig. 4b.

The scanned and pre-processed point cloud achieved a very high surface point density, with a distribution of 345 pts/m². This distribution of point cloud density is

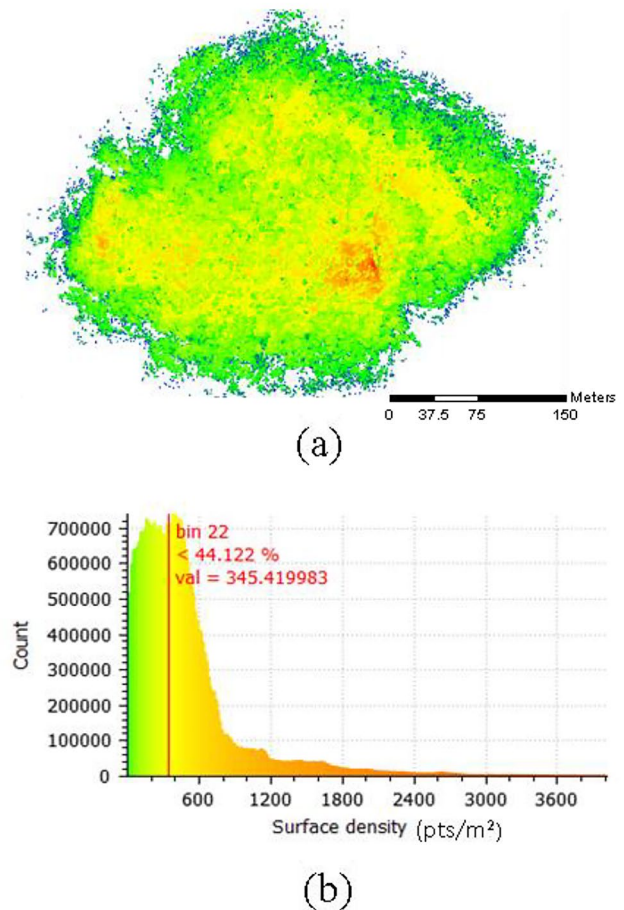


Fig. 4 a Surface point density map obtained through UAV-LiDAR survey of the study area and b Histogram distribution of the surface point density - also showing the colour scale

significantly higher than what was traditionally achieved through airborne surveys (approx. 20–40 pts/m²). This means UAV-LiDAR metrics can be produced with a significant accuracy and detail, which is beneficial to identifying and distinguishing the complex distribution of vegetation communities in a diverse ecosystem area such as swamps. Furthermore, high point density increases the likelihood of more points being recovered from under the canopies, which is essential to produce an accurate topographical surface model to identify any deformation induced from underground longwall mining. This indicates the potential benefit of using a UAV-LiDAR system in environmental applications requiring fine-scale mapping.

The pre-processing steps to filter the point cloud are also essential to avoid propagating errors in the LiDAR metrics. A synoptic overview of the pre-processed point cloud is shown in Fig. 5. A false coloured composite of the processed LiDAR metrics (kurtosis, maximum vegetation height and coefficient of variation) for a spatially subset region is shown in Fig. 5a without any pre-processing and in Fig. 5b with proper pre-processing. The comparison demonstrated the efficacy of the pre-processing phase to avoid erroneous artefacts in the processed false coloured composite of the LiDAR metrics, marked in white ovals; such artefacts are removed with pre-processing.

3.3 LiDAR metrics

The point cloud from the UAV-LiDAR survey was processed to produce a total of 35 LiDAR metrics related to topography, vegetation structure and intensity. The computed metrics are equivalent to raster products, which can differentiate different vegetation species and classes using classical classification workflows and provide information related to swamp vegetation conditions. A few of the selected maps of LiDAR metrics such as local roughness, slope cosine aspect (Slpcosasp), height range, vegetation cover, foliage height density (FHD), and mean intensity are shown in Fig. 6. The swamp area can be visually distinguished from the surrounding terrestrial type *Eucalyptus* trees without further processing. This shows the potential of a high-density point cloud obtained through the UAV-LiDAR survey.

3.4 Canopy height model

The UAV-LiDAR point cloud was processed to produce a canopy height model (CHM) of the swamp environment. A CHM is useful for characterising the extent of an upland swamp environment by differentiating the low-lying peat swamp vegetation from the surrounding terrestrial vegetation such as *Eucalyptus* trees (Jenkins and Frazier 2010). A

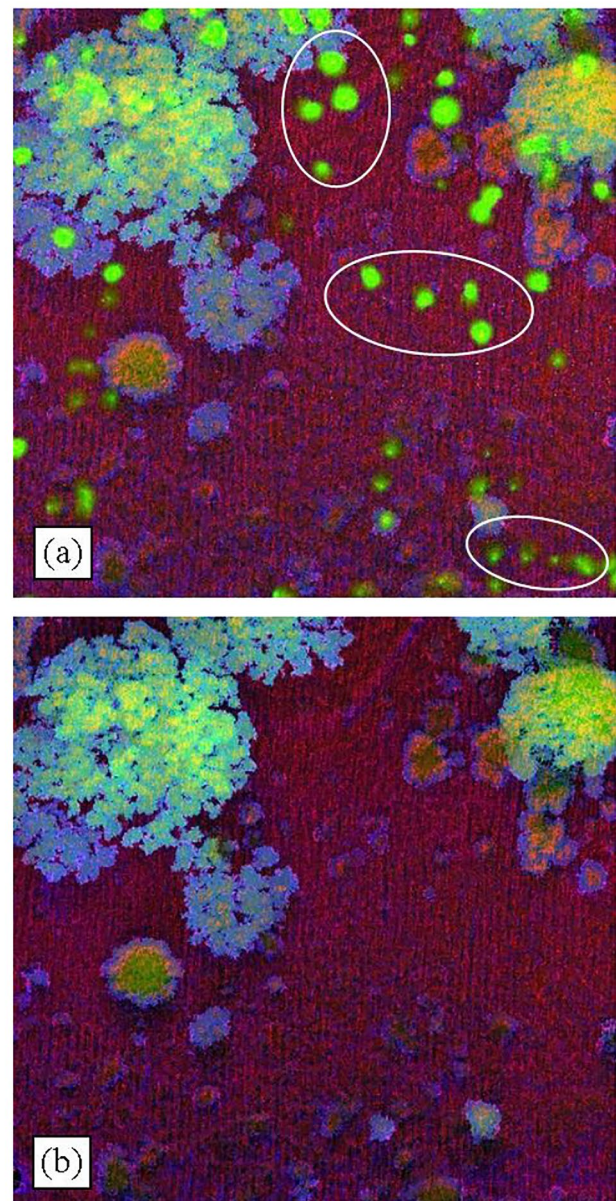


Fig. 5 Pre-processed point cloud (coloured as per elevation), and false colour composite (kurtosis, maximum vegetation height and coefficient of variation) of LiDAR matrices for a subset area: **a** Without pre-processing and **b** With pre-processing

colour scaled synoptic view of the CHM for the two swamp sites in the study area is shown in Fig. 7a and a textured three-dimensional view is shown in Fig. 7b. The accuracy of the CHM was analysed with the ground truth values of canopy height measurements for shrub-type swamp vegetation cover. The overall R^2 accuracy was found to be approximately 0.76, which was deemed sufficient for the type of vegetation cover. The computation of accurate CHM for shrub-type vegetation is relatively difficult compared to tree-type vegetation cover. This depends on two factors: the

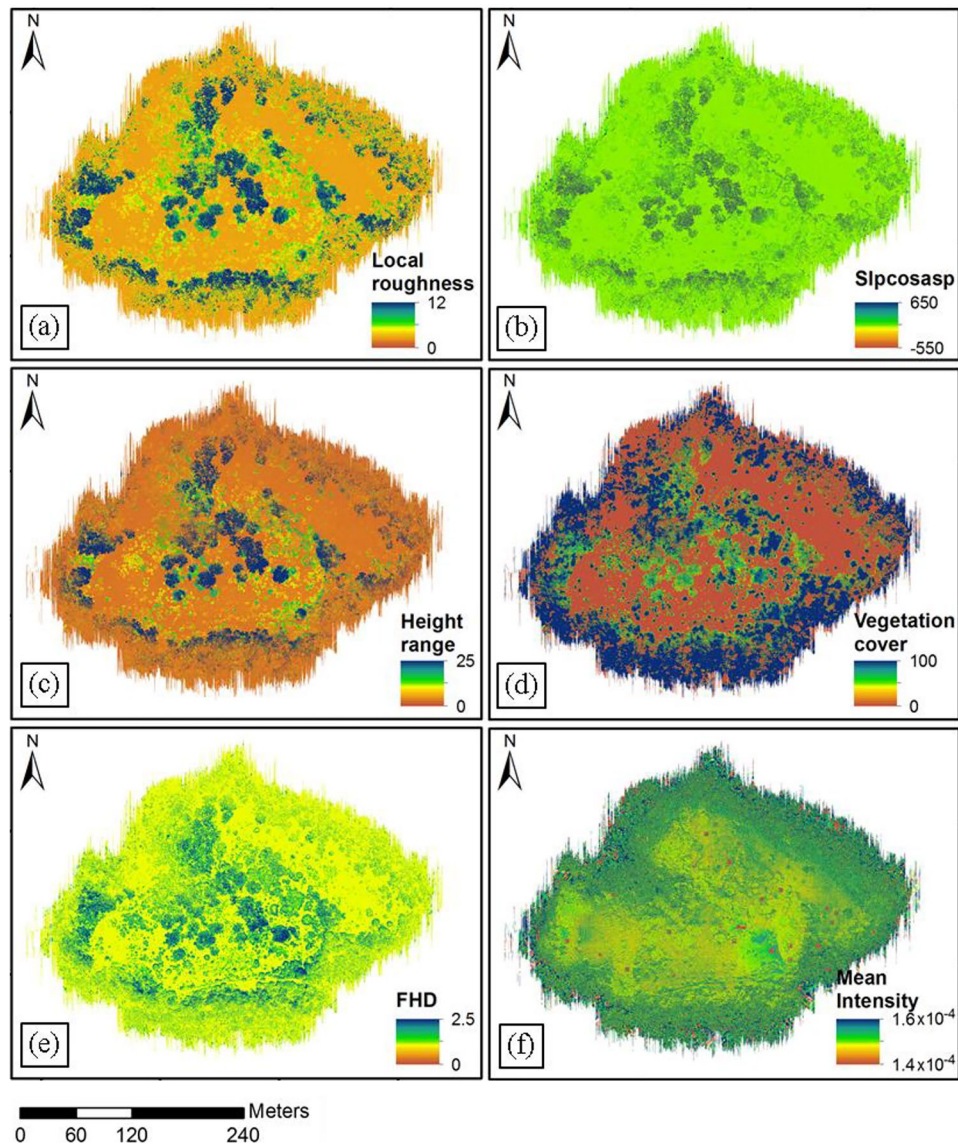


Fig. 6 LiDAR metrics maps of **a** Local roughness; **b** Slope cosine aspect (Slpcosasp); **c** Height range; **d** Vegetation cover; **e** Foliage height density (FHD) and **f** Mean intensity

small and fragile nature of shrub-type vegetation canopies, and the footprint size of the laser. Under these scenarios, the accuracy of models could be improved by improving the beamwidth of the internal laser sensor in the UAV-LiDAR system or by incorporating machine learning methods to perform a parametric transformation of the coarse CHM product using reference tie point measurements.

3.5 Classification of vegetation communities

Data collected using the UAV-LiDAR system was evaluated using a classification-based approach. The respective

datasets were collected for both swamp site-1 and site-2. A total of eight vegetation classes as described in Sect. 2.1 were present in swamp site-1 and site-2, these eight vegetation classes were used to operate the classification based evaluation, i.e. Dagger hakea, Grass tree, Heath-leaved banksia, Black sheoak, Bracken fern *Eucalyptus* tree, Pouched coral fern and Sedgeland complex. Additionally, some portion of the imaged area comprised of no-vegetation cover and was treated as a separate ‘Bare earth’ class, i.e., a total of nine classification classes. The UAV-LiDAR metrics were dimensionally reduced using PCA and ICA, both of which were used for comparative analysis. The overall

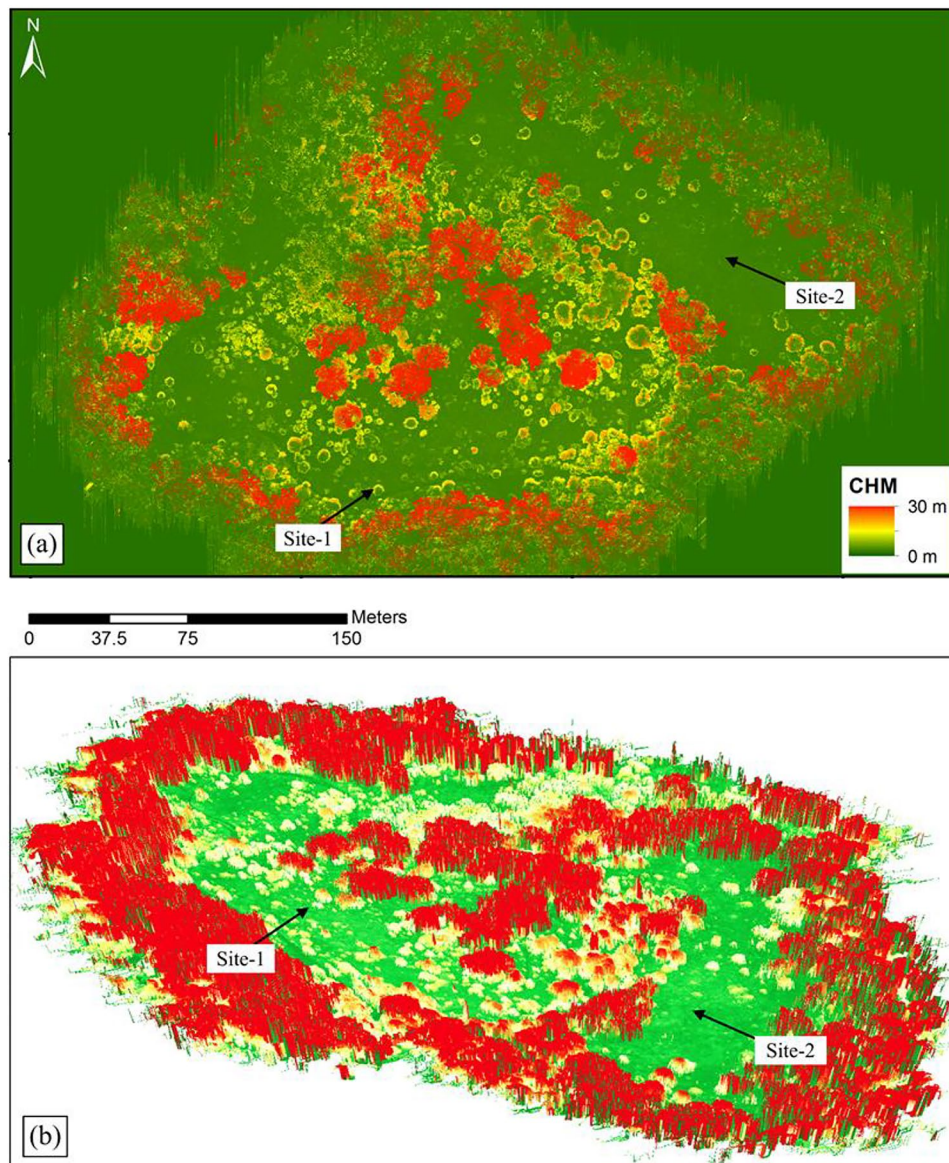


Fig. 7 Canopy height model of the study area: **a** Synoptic view and **b** Textured three-dimensional view

accuracy and kappa coefficient of the methods are listed in Table 2. The ICA(LiDAR) marginally outperformed the PCA(LiDAR) with most classifiers, with the exception of PP and SID. The best classification result was produced by combining the ICA(LiDAR) data with SVM classifier, which produced an overall accuracy of 73.42% and a kappa coefficient of 0.64.

4 Discussion

4.1 Integration of UAV-LiDAR system

The UAV-LiDAR system was developed through sensor and platform integration, including sensor calibration, sensor operation, orientation, mission planning, and data acquisition. The installation of a LiDAR sensor on the UAV required thorough consideration of several aspects of sensor parameters such as laser range, GPS and IMU accuracy, beamwidth, a scanning mechanism, field-of-view and angle

Table 2 Accuracy assessment for the classification of UAV-LiDAR data

Classifier	PCA (LiDAR)		ICA (LiDAR)	
	Overall accuracy (%)	Kappa	Overall accuracy (%)	Kappa
Parallelepiped (PP)	18.49	0.13	5.91	0.04
Maximum Likelihood (ML)	58.77	0.49	60.00	0.51
Minimum Distance (MD)	43.16	0.33	45.49	0.35
Mahalanobis Distance (MHD)	48.02	0.37	48.31	0.38
Spectral Angle Mapper (SAM)	43.73	0.33	45.49	0.35
Spectral Information Divergence (SID)	46.84	0.37	32.08	0.23
Support Vector Machine (SVM)	73.37	0.64	73.42*	0.64*

* Best result

The producer's and user's accuracy for each class with the best classification method is shown in Table 3. The classification accuracy was high for bare earth, Dagger hakea, Black sheoak, *Eucalyptus* trees and Sedgeland complex. However, the accuracy for Grass tree, Heath-leaved banksia, Bracken fern and Pouched coral fern was exceptionally low. The low accuracy with these classes for LiDAR is not surprising since the structural characteristics of these species are indistinguishable through LiDAR point cloud. The accuracy was high for tall terrestrial trees such as Black sheoak and *Eucalyptus*, which improved the classification accuracy of the Sedgeland complex class. The classification maps for and ICA(LiDAR) based approach using SVM classifier is shown in Fig. 8

of scanning. The mission planning focused on these sensor parameters to obtain an accurate point cloud with high surface point density, which required a design of a suitable calibration loop, and flight paths with significant overlap of laser footprints in both along and across-track directions. Attention and diligence to these aspects of system integration and operation were essential to retrieve accurate and effective data products seamlessly. Overall, these considerations and innovative tuning towards various design and integration phases are critical to mine environmental monitoring, and other applications requiring accurate thematic mapping with UAVs, such as agriculture, forestry.

Table 3 Class wise accuracy of best classification method – ICA(LiDAR) with support vector machine

Class	Producer's accuracy (%)	User's accuracy (%)
Bare earth	78.12	82.88
Dagger hakea	99.17	92.07
Grass tree	16.95	32.51
Heath-leaved banksia	11.02	62.22
Black sheoak	87.35	73.18
Bracken fern	40.23	50.75
<i>Eucalyptus</i> tree	80.67	91.25
Pouched coral fern	58.68	52.45
Sedgeland complex	94.85	64.06

4.2 High-resolution point cloud from UAV-LiDAR

Acquisition of high-density point cloud is essential for detailed 3D imaging of the environment. Several factors such as speed of UAV-LiDAR system during scanning, distance from the target or flying height, spacing between transects and across track scan width influences the density of points collected during a scan. Furthermore, quality influencing factors such as uncertainty in altitude, position error, number of available satellites, and differential lag need to be controlled to obtain well-registered point cloud data. A workflow was devised through the combination of a set of different software and processing solutions to effectively convert raw LiDAR return, position, orientation and quality information to a point cloud with high surface density, to pre-process the point cloud to remove redundant points and IMU induced errors, and to prepare the point cloud for further processing. The geometric accuracy of the integrated UAV-LiDAR system is crucial for fine-scale monitoring and mapping applications. A dedicated geometric quality assessment exercise confirmed the high accuracy of the system. The system produced a very high-density point cloud in the complex swamp environment, which was helpful for the differentiation of several vegetation types.

4.3 Derived LiDAR metrics

The complex assemblage of swamp vegetation species and communities was studied using a UAV-based LiDAR system. A total of 35 LiDAR metrics related to topography, vegetation structure and intensity were produced. The computed metrics are raster products similar to hyperspectral indices, which can differentiate different vegetation species and communities using a classical classification workflow and provide useful information on swamp vegetation conditions. The vegetation indices and selected LiDAR metrics produced through the UAV survey were validated and cross-validated against biophysical parameters such as leaf area index (LAI) and canopy height model (CHM).

Deriving LiDAR metrics from a high-density point cloud is a computationally-intensive process. To provide an estimate, a spatial subset of the point cloud of approximately one-tenth the size of the total point cloud at a point density of 345 pts/m² took over a week of processing to produce LiDAR metrics at 2 cm of resolution. This order of computational inefficiency is limiting for routine environmental monitoring operations. Nevertheless, LiDAR metrics could be relatively easily generated at lower spatial resolutions (> 10 cm). However, reconstruction of a multi-core parallel computation pipeline for the generation of LiDAR metrics, could be future scope for fine-scale mapping applications using UAV-LiDAR.

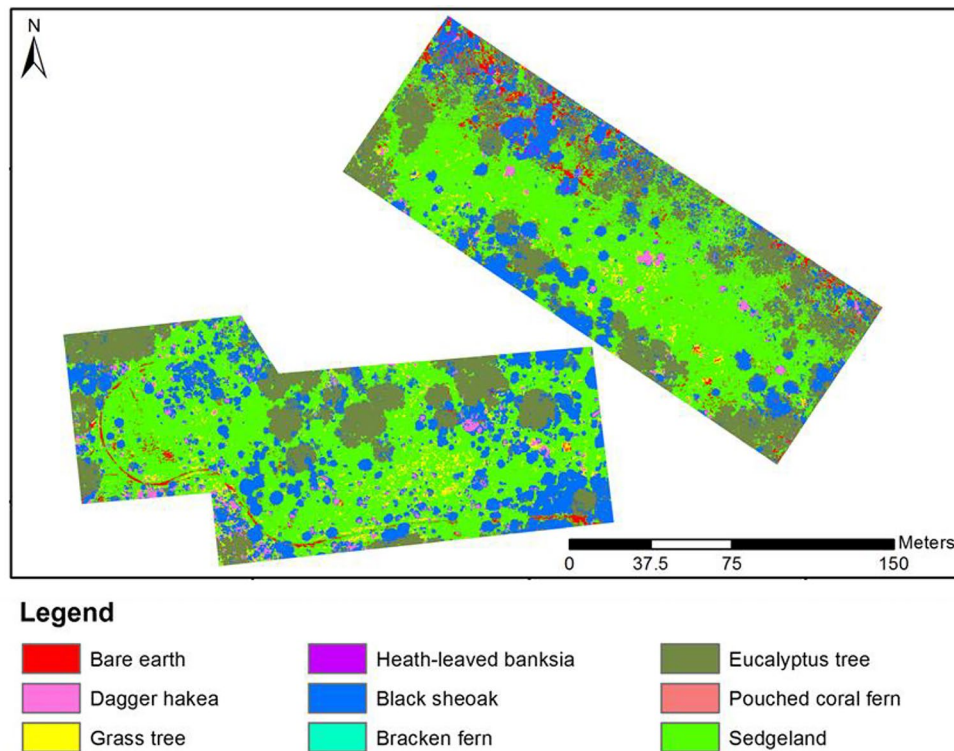


Fig. 8 Classification map of swamp site-1 and site-2 vegetation classes and species produced with **a** UAV-hyperspectral and **b** UAV-LiDAR data, using support vector machine classifier

4.4 Monitoring vegetation communities using UAV-LiDAR

Satellite based spectral monitoring has been used to differentiate bog from surrounding surface covers, such as sedge lands or grasslands, and identify any gain or loss in woody vegetation (Lechner et al. 2012). Such methods effectively monitor swamps if the phenology of the vegetation is documented, and especially, if changes in phenology due to presence or absence of water is known (CoA 2014). Natural fluctuations in variability over time are indicative of growth rates and phenology which could be analysed using remote sensing images of wet and dry seasons. Existing phenology products such as Australian Phenology Product available from Terrestrial Ecosystem Research Network (TERN) is coarse (5.6 km) in resolution and limited to regional level ecosystem modelling. THPSS sites represent small patches of the diverse ecosystem, which limits the applicability of readily available regional phenology products. Ground-based phenological survey products could not be found for the study area. By developing appropriate UAV-based sensing systems, this study acts as a foundation to generate fine-scale vegetation maps through UAV-based remote sensing surveys in the future.

Within the Sedgeland-complex class, the composition of species varies from one region in the swamps to another,

and these subtle variations result in homogenous to heterogeneous conglomerations of target species as different sub-categories. Banerjee et al. (2017) identified the challenges in classifying these sub-categories of the Sedgeland complex as distinct classes due to the scale at which these species are mixed together, resulting in complex spectral and structural intermixing. However, it was essential to treat these sub-categories distinctly for biophysical parameter retrieval. Hence, the species composition mapping through further investigations has been performed using UAV-hyperspectral; however, only spectral information was insufficient in accurately mapping complex assemblages of species in swamp environments (Banerjee et al. 2020). Therefore, this study investigated the potential of LiDAR as a structural modality in mapping vegetation communities in diverse ecosystems. Additionally, the classification maps produced with the UAV-LiDAR system are less prone to shadow effects than optical and hyperspectral datasets. In future, a fusion-based approach between UAV based hyperspectral and LiDAR datasets could be valuable in accurately mapping complex vegetation communities.

5 Conclusions

Traditional satellite and airborne remote sensing have been widely used tools in scientific research and environmental monitoring at global and regional levels. Its adoption in fine-scale monitoring and mapping related applications has been challenging due to limited spatial resolution, atmospheric noise and cloud cover. The advent of near-earth imaging systems such as UAV-LiDAR has offered the potential for detailed mapping and monitoring of landcover units. Although these systems are popular in allied disciplines such as agriculture and forestry, their application for monitoring complex ecosystems and environments such as swamps has been limited. This is partly due to the absence of an existing methodological framework and challenges in using UAV-based sensor systems in these sensitive and complex environments. The primary objective of this research was to develop a functional UAV-based LiDAR sensing system, including a workflow to generate accurate datasets and products for environmental monitoring applications. A critical review was undertaken to identify the current state and limitations of UAV-based LiDAR technologies for mine environmental monitoring research. Several issues that make effective use of these technologies challenging for seamless data generation and processing were identified and resolved, leading to the classification of complex vegetation communities in sensitive ecosystems. The technology and methodology demonstrated herein would be potentially valuable in identifying changing conditions or the health of ecosystems. The UAV-LiDAR system would be valuable for mapping the composition of THPSS vegetation communities at an unprecedented scale and accuracy. Future research would also include investigating machine learning and deep learning classification algorithms to improve the delineation of vegetation species and communities.

Author contributions B.P.B. conceived the experiment, conducted the experiments, performed data analysis and drafted the original manuscript. S.R. assisted in developing the concept of the study, completed the project administration, provided supervision and reviewed and edited the manuscript. All authors reviewed the manuscript. All authors have read and agreed to the published version of the manuscript.

Funding No funding was received to assist with the preparation of this manuscript.

Declarations

Financial interests The authors declare they have no financial interests.

Conflict of interest The authors declare no conflicts of interest.

Open Access This article is licensed under a Creative Commons Attribution 4.0 International License, which permits use, sharing,

adaptation, distribution and reproduction in any medium or format, as long as you give appropriate credit to the original author(s) and the source, provide a link to the Creative Commons licence, and indicate if changes were made. The images or other third party material in this article are included in the article's Creative Commons licence, unless indicated otherwise in a credit line to the material. If material is not included in the article's Creative Commons licence and your intended use is not permitted by statutory regulation or exceeds the permitted use, you will need to obtain permission directly from the copyright holder. To view a copy of this licence, visit <http://creativecommons.org/licenses/by/4.0/>.

References

- Akcil A, Koldas S (2006) Acid Mine Drainage (AMD): causes, treatment and case studies. *J Clean Prod* 14(12):1139–1145
- Banerjee BP, Raval S (2021) A Particle Swarm Optimization Based Approach to Pre-Tune Programmable Hyperspectral Sensors. *Remote Sens* 13(16):3295
- Banerjee BP, Raval S, Cullen PJ (2017) High-resolution mapping of upland swamp vegetation using an unmanned aerial vehicle-hyperspectral system. *J Spectr Imaging* 6(1):a6
- Banerjee BP, Raval S, Cullen PJ (2020) UAV-hyperspectral imaging of spectrally complex environments. *Int J Remote Sens* 41(11):4136–4159. doi:<https://doi.org/10.1080/01431161.2020.1714771>
- Banerjee BP, Raval S, Cullen PJ, Shen XJ (2018) Mapping of complex vegetation communities and species using uav-lidar metrics and high-resolution optical data. Paper presented at the 38th annual symposium of IEEE International Geoscience and Remote Sensing Symposium, Valencia, Spain
- Cameron AC, Windmeijer FA (1997) An R-squared measure of goodness of fit for some common nonlinear regression models. *J Econ* 77(2):329–342
- CoA (2014) Temperate Highland Peat Swamps on Sandstone: ecological characteristics, sensitivities to change, and monitoring and reporting technique. Independent Expert Scientific Committee on Coal Seam Gas and Large Coal Mining Development, Department of the Environment, Australian Government
- Colomina I, Molina P (2014) Unmanned aerial systems for photogrammetry and remote sensing: A review. *ISPRS J Photogrammetry Remote Sens* 92(0):79–97. doi:<https://doi.org/10.1016/j.isprsjprs.2014.02.013>
- Congalton RG (1991) A Review of Assessing the Accuracy of Classifications of Remotely Sensed Data. *Remote Sens Environ* 37(1):35–46 doi:[https://doi.org/10.1016/0034-4257\(91\)90048-B](https://doi.org/10.1016/0034-4257(91)90048-B)
- Englhart S, Jubanski J, Siegert F (2013) Quantifying dynamics in tropical peat swamp forest biomass with multi-temporal LiDAR datasets. *Remote Sens* 5(5):2368–2388
- Gandaseca S, John S, Haruna Ahmed O, Muhamad N (2009) Vegetation assessment of peat swamp forest using remote sensing. *Am J Agricultural Biol Sci* 4(2):167–172
- Greene R, Timms W, Rengasamy P, Arshad M, Cresswell R (2016) Soil and aquifer salinisation: Toward an integrated approach for salinity management of groundwater. In: Jakeman AJ, Barretreau O, Hunt RJ, Rinaudo JD, Ross A (Eds), *Integrated Groundwater Management*. Springer, pp 377–412. doi:https://doi.org/10.1007/978-3-319-23576-9_15
- Hyvärinen A, Oja E (2000) Independent component analysis: algorithms and applications. *Neural Netw* 13(4):411–430
- Jaakkola A, Hyypä J, Kukko A, Yu X, Kaartinen H, Lehtomäki M, Lin Y (2010) A low-cost multi-sensor mobile mapping system and its feasibility for tree measurements. *ISPRS J*

- Photogrammetry Remote Sens 65(6):514–522. doi:<https://doi.org/10.1016/j.isprsjprs.2010.08.002>
- Jenkins RB, Frazier PS (2010) High-resolution remote sensing of upland swamp boundaries and vegetation for baseline mapping and monitoring. *Wetlands* 30(3):531–540. doi:<https://doi.org/10.1007/s13157-010-0059-1>
- Lechner AM, Fletcher A, Johansen K, and Erskine P (2012) Characterising upland swamps using object-based classification methods and hyper-spatial resolution imagery derived from an Unmanned Aerial Vehicle. XXII ISPRS Congress, Technical Commission IV, Melbourne, Australia, 25 August-01 September 2012. Melbourne, Australia: ISPRS. doi:<https://doi.org/10.5194/isprsannals-I-4-101-2012>
- Lin Y, Hyyppä J, Jaakkola A (2011) Mini-UAV-borne LIDAR for fine-scale mapping. *IEEE Geosci Remote Sens Lett* 8(3):426–430
- Lopes A, Touzi R, Nezry E (1990) Adaptive speckle filters and scene heterogeneity. *IEEE Trans Geosci Remote Sens* 28(6):992–1000
- The Native Vegetation of the Woronora, O'Hares and Metropolitan Catchments (2003) NSW National Parks and Wildlife Service (NPWS)
- NSWDP (2008) Impacts of Underground Coal Mining on Natural Features in the Southern Coalfield: Strategic Review. Sydney, NSW, Australia
- Opitz J, Timms W (2016) Mine water discharge quality—a review of classification frameworks
- Ren H, Zhao Y, Xiao W, Hu Z (2019) A review of UAV monitoring in mining areas: current status and future perspectives. *Int J Coal Sci Technol* 6(3):320–333. doi:<https://doi.org/10.1007/s40789-019-00264-5>
- Richards JA, Richards J (1999) Remote sensing digital image analysis, vol 3. Springer
- Setiawan Y, Pawitan H, Prasetyo L, Permatasari P (2017) Monitoring tropical peatland ecosystem in regional scale using multi-temporal MODIS data: Present possibilities and future challenges. In: IOP Conference Series: Earth and Environmental Science, vol 1. IOP Publishing, p 012052
- Setiawan Y, Pawitan H, Prasetyo LB, Parlindungan M, Permatasari PA (2016) TEMPORAL VEGETATION : A MONITORING APPROACH OF HIGH-SENSITIVE ECOSYSTEM IN REGIONAL SCALE. *Geoplanning: Journal of Geomatics and Planning* 3 (2):137–146
- Strecha C, Fletcher A, Lechner A, Erskine P, Fua P (2012) Developing species specific vegetation maps using multi-spectral hyperspatial imagery from unmanned aerial vehicles. *ISPRS Annals of the Photogrammetry, Remote Sensing and Spatial Information Sciences* 3:311–316
- Streutker DR, Glenn NF (2006) LiDAR measurement of sagebrush steppe vegetation heights. *Remote Sens Environ* 102(1):135–145
- Vervoort A (2021) Various phases in surface movements linked to deep coal longwall mining: from start-up till the period after closure. *Int J Coal Sci Technol* 8(3):412–426. doi:<https://doi.org/10.1007/s40789-020-00325-0>
- Wallace L, Lucieer A, Watson CS (2014) Evaluating tree detection and segmentation routines on very high resolution UAV LiDAR data. *IEEE Trans Geosci Remote Sens* 52. doi:<https://doi.org/10.1109/TGRS.2014.2315649>
- Younger PL, Wolkersdorfer C (2004) Mining impacts on the fresh water environment: technical and managerial guidelines for catchment scale management. *Mine Water Environ* 23:s2–s80
- Zhang Z, Li Z, Tian X (2018) Vegetation change detection research of Dunhuang city based on GF-1 data. *Int J Coal Sci Technol* 5(1):105–111. doi:<https://doi.org/10.1007/s40789-018-0195-4>

Publisher's note Springer Nature remains neutral with regard to jurisdictional claims in published maps and institutional affiliations.